Diagnosis of Two-Phase Oil/Gas Flow in a Closed Pipe using an 8-Electrode ECT System

Sidi Mohamed Ahmed Ghaly
Electrical Engineering Department, Imam Mohammad Ibn Saud Islamic University, Saudi Arabia | Ecole Normale Supérieure, Mauritania
smghaly@imamu.edu.sa

Mohammed Shalaby
Electrical Engineering Department, Imam Mohammad Ibn Saud Islamic University, Saudi Arabia
myshalaby@imamu.edu.sa

Mohammad Obaidullah Khan
Electrical Engineering Department, Imam Mohammad Ibn Saud Islamic University, Saudi Arabia
okkhan@imamu.edu.sa

Khaled Alsnaie
Electrical Engineering Department, Imam Mohammad Ibn Saud Islamic University, Saudi Arabia
kalsnaie@imamu.edu.sa

Asad Ali Mohammed
Electrical Engineering Department, Imam Mohammad Ibn Saud Islamic University, Saudi Arabia
asad207@imamu.edu.sa

Faisal Baloshi
Electrical Engineering Department, Imam Mohammad Ibn Saud Islamic University, Saudi Arabia
fbaloshi@imamu.edu.sa

Abdalmajid Imad
Electrical Engineering Department, Imam Mohammad Ibn Saud Islamic University, Saudi Arabia
aimad@imamu.edu.sa

Majdi Taha Oraiqat
Electrical Engineering Department, Imam Mohammad Ibn Saud Islamic University, Saudi Arabia
mtoraiqat@imamu.edu.sa

Received: 4 May 2023 | Revised: 24 May 2023 and 26 May 2023 | Accepted: 29 May 2023

 DOI: https://doi.org/10.48084/etasr.6011

ABSTRACT

Electrical tomography techniques have been developed to monitor the internal behavior of industrial processes. Electrical capacitance gives the best benefits over other tomography modalities, as it has no radiation, is non-intrusive, and has a low cost. This study investigated the diagnosis of two-phase oil/gas flow in a closed pipe, using an image data capture system for an 8 external electrode Electrical Capacitance Tomography (ECT) sensor. The system had a high-resolution ratio, a small measurement error, and was able to remove the effects of stray capacitance. Experimental measurements were carried out on two different materials that filled the space inside the pipe in different proportions to determine the sensitivity and accuracy of the measurement. The results showed that the system had fast image data capture time, high accuracy, a very small resolution ratio, and a good signal-to-noise ratio and quality factor.

Keywords-ECT sensor; imaging; electrode; permittivity; fluid dynamics; sensitivity; accuracy

I. INTRODUCTION

Electrical Capacitance Tomography (ECT) is a widely used imaging technique in monitoring and diagnosing the internal dynamics of the flow mechanism of gaseous or liquid materials in the process industry [1-5]. ECT is an economic, non-interrupting or non-invasive, and fast-responding imaging scheme, as it can produce real-time images with an approximate speed of 100 fps. Different experimental studies showed that the Water-in-Liquid Ratio (WLR) and Gas Volume Fraction (GVF) in an oil-gas-water flow can be roughly calculated or measured by ECT with suitable algorithms [6-7]. Obtaining a high-speed image along with quantitative measurements of a multiphase flow system is a challenging demand in the petroleum industry and hydraulic applications. ECT can also be used to detect corrosion and leakage or monitor liquid dynamics in a petroleum/gas pipeline network [8-10]. It can also be used to investigate the distribution of spatial permittivity in a defined region in the interior of a closed pipe. ECT works on the principle of measuring capacitances between electrodes located outside the sample portion in the region of investigation. In general, the specimen region can be a hollow pipe carrying a liquid or gas. The data obtained from these electrodes are processed to reconstruct the internal image of the pipe. The necessary elements of a typical ECT system are a set of multi-electrode sensors mounted equidistant around the pipe, a data retrieval or acquisition system, and an image reconstruction block, as shown in Figure 1 [11-12]. Using N electrodes in the sensor for capacitance measurements, there will be M independent capacitance measurements as expressed in:

$$M = \frac{N\,(N-1)}{2} \quad (1)$$

In the present case, as shown in Figure 2, an 8-electrode sensor needs 28 independent measurements of electrode pairs as:1-2, 1-3, ..., 1-8; 2-3, 2-4, ..., 2-8; ..., up to 7-8.

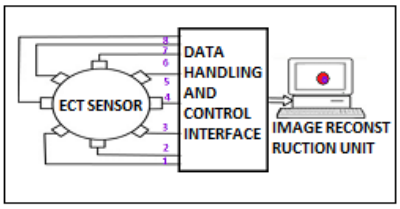

Fig. 1. A typical ECT system with 8 electrodes.

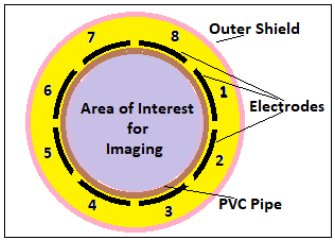

Fig. 2. Cross section of a typical 8-electrode ECT system.

In general, ECT systems directly employ the "raw" capacitance data obtained from the sensor to develop images using Linear Back-Projection (LBP) and recursive or neural network algorithms [10]. The LBP algorithm is one of the most popular methods due to its simplicity and high rates of image reconstruction. An LBP image is obtained by overlaying the sensor sensitivity maps for all electrode pairs after weighting by the corresponding measured changes in normalized capacitance. This can be represented mathematically as:

$$X(p) = \frac{\sum_{i=1}^{N-1}\sum_{j=i+1}^{N}\lambda_{ij}S_{ij}(p)}{\sum_{i=1}^{N-1}\sum_{j=i+1}^{N}Sij(p)} \quad (2)$$

$$\lambda_{ij} = \frac{c_{ij}^{m}-c_{ij}^{l}}{c_{ij}^{h}-c_{ij}^{l}} \quad (3)$$

where N represents the number of electrodes in the ECT sensor, $X(p)$ is the fraction of a high permittivity material in the p-th pixel, S is the sensitivity of electrode pair i-j at the p-th pixel, C_{ij} represents the capacitance of the electrode pair i-j when the sensor is filled with low and high permittivity materials, respectively, c^m is the raw measured capacitance of the electrode pair i-j, and λ_{ij} is the change in normalized capacitance of the respective electrode pair.

II. ELECTRICAL MODELING OF THE ECT SENSOR WITHOUT RADIAL SCREEN

Consider an ECT sensor with eight external electrodes without radial screens, as shown in Figure 2. These electrodes can be made with a flexible printed circuit board with greater precision in size and position. Without radial screens, the external capacitances must be considered, as they have considerable capacitance. A model of capacitance measured C_m with radial screens for one pair of electrodes, that is the capacitance between two measurement electrodes through the space outside them, can be given as the combination of an internal capacitance C_x, two pipe wall capacitances C_{w1}, C_{w2}, and two stray capacitances C_{s1}, C_{s2}, as demonstrated in Figure 3(a). This can be further simplified as shown in Figure 3(b) [13]. The equivalent capacitance C_m can be calculated mathematically as:

$$Cm = \frac{Cw\,Cx}{Cw+Cx} \quad (4)$$

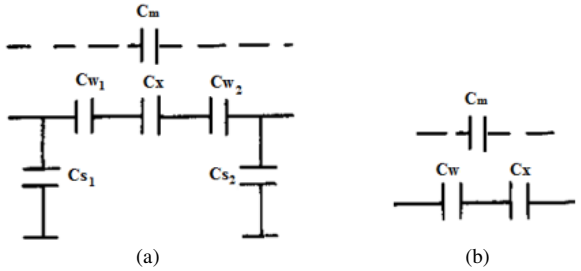

Fig. 3. Electrical Model of 8-electrode sensing system without radial screen: (a) Model with all capacitances, (b) simplified model.

The unknown capacitances C_w and C_x can be found by filling a material of known relative permittivity ε_{r1} into the sensor. This process is repeated with another material of known

relative permittivity of ε_{r2} and the air. Thereafter, by finding C_x and C_w, the internal capacitance with any fluid existing inside the region of interest in the PVC pipe can be calculated from the raw capacitance measured using (4). This can be rearranged as follows:

$$C_x = C_w\, C_m/(C_w - C_m) \quad (5)$$

III. CALCULATION OF THE SENSITIVITY MAP OF THE 8-ELECTRODE ECT

Consider the circular sensor filled with one-phase with air dielectric constant and fitted with eight electrodes. The wall permittivity is constant. Thus, the domain of the model is the unit square Ω on the x-y plane, representing the cross-section of the scaled sensor area. The electrodes are placed on the unit square x^2=1, where x is the length of the side and the boundary of Ω. Suppose that the relative radial thickness of the wall is t_0 ($0<t_0<1$), and denotes the interior cavity by [14-15]:

$$\Omega_0 = \{(x, y): x^2 < (1 - t_0)^2\} \quad (6)$$

The electric potential $u(x, y)$ on Ω is governed by Poisson's equation derived for the static electric field, which is given by:

$$\nabla(\varepsilon\nabla u) = 0\Omega \quad (7)$$

where $\varepsilon = \varepsilon(x, y) > 0$ is the relative permittivity distribution in Ω. A finite difference method was employed to discretize the differential equation for the numerical solution using rectangular coordinates.

The simulation was assumed for a cross-sectional circular shape, which can be a cylindrical non-metal container. ECT is difficult to perform on metallic cylinders, as the metals leak the charge all over their surface and make the theoretic assumptions wrong for calculations. On a non-metallic surface, the electrodes are attached and a voltage is applied, which passes through the non-metallic cylinder from the inside and through the fluid or gas. This creates a small charge that accumulates in the fluid or gas and creates a small capacitance since when a potential is applied to one electrode, the other 7 electrodes act as ground. The technique of 8-electrode ECT is like 7 capacitors along the surface of the cylinder. However, as the permittivity and voltage between the plates are very small and the distance between the electrodes is greater, a very low capacitance is measured. If the permittivity of the fluid or gas and their potential breakdown are known, an increase in voltage below the breakdown voltage can lead to better performance of the ECT technique. The breakdown voltage is the voltage at which an arc occurs between the electrodes. Figure 4 shows the electric potential between the energized electrode 1 and the grounded electrodes 2-8. The sensitivity map S_{ij} is obtained on a cylinder object fixed with 8 electrodes. Figure 5 shows S_{12} between the first and second electrodes. Electrode 1 is energized at a low voltage of 0.02 V and electrode 2 is grounded, which has some stray charge on it, as the metal electrodes cannot be charged after applying an electric field. Similarly, electrode 1 is energized at a low voltage of 0.02 V, and electrode 3 is grounded having some stray charge. The potentials for electrodes 1 and 3 are illustrated below. This can be demonstrated for all combinations of 1-8 electrodes in the ECT sensor, as shown in Figure 6. Figure 7 shows S_{13} between the first and third electrodes.

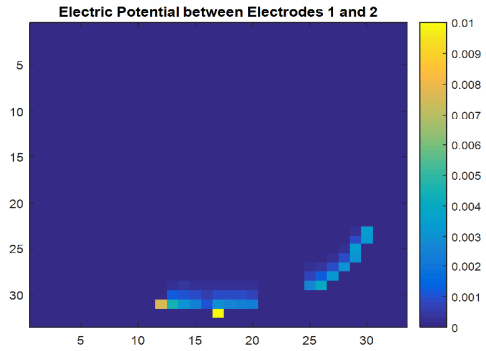

Fig. 4. Electric Potential between Electrodes 1 and 2.

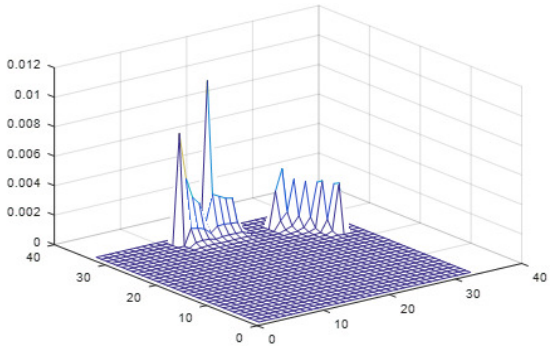

Fig. 5. Sensitivity map between electrodes 1 and 2.

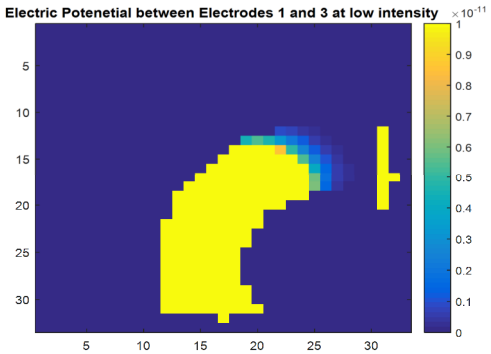

Fig. 6. Electric potential between electrodes 1 and 3 at low intensity.

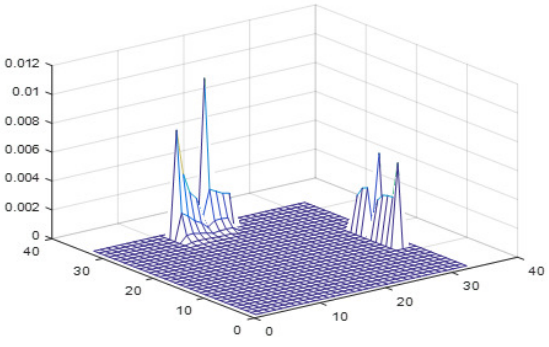

Fig. 7. Sensitivity map between electrodes 1 and 3.

Figure 8 illustrates the potential distribution from electrode 1 to electrode 3 when a high voltage of 1000 V is applied. If carefully analyzed, there is a continuous decrease in voltage until the second electrode is approached. It seems as an exponential decrease in voltage, but when applying a higher voltage at electrode 1, a more positive expectation of capacitance is measured. The application of higher voltage is due to the limitation of the medium which is transmitted through the cylindrical pipes, and its effect needs to be studied.

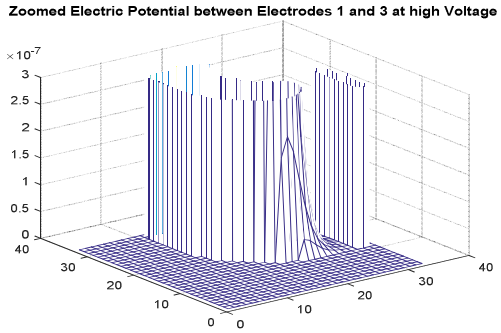

Fig. 8. Electric potential between electrodes 1 and 3 at high voltage.

IV. IMPLEMENTATION FOR SENSITIVITY MEASUREMENT

The AC-ECT system includes hardware and software, in particular software drivers and ECTGUI. As shown in Figure 9, the hardware has a front-end unit in a 19" Eurocase, with an internal power supply and an NI DAQ board/card operated by a host PC. Two NI DAQ units are supported: the NI PCI-6024E DAQ board that works with a desktop PC and the NI PCMCIA 6062E DAQ card that works with a laptop. Both NI DAQ units use a 68-way ribbon cable with the same female connectors connected to the 19" Eurocase, but a different female connector at the other end to connect to the PC [16].

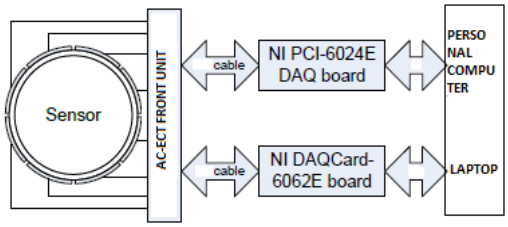

Fig. 9. Hardware blueprint.

This section presents the results of the experiments carried out using the 8-electrode ECT sensor, with dimensions specified in Table I, to quantify its sensitivity. The accuracy of the sensor may also depend on physical specifications and assumptions. If the tube wall is made up of a dielectric material, electrodes can be installed inside or outside [17-18], but if the wall is conductive there is only one choice to design the electrode location (external electrode). However, as the proposed design used dielectric material, the electrodes were put outside the pipe because it is easier to design. The number of electrodes depends on capacitance, circuit complexity, and data acquisition speed. Using more electrodes provides a better image, but they are difficult to measure. In most cases, the number of electrodes used is 8 or 12, whereas this study used 8. A guard electrode is required to improve measurement sensitivity and prevent the electric field from reaching the ground and the end of the measuring electrode [19]. They must be used if the length of measuring electrodes is less than approximately twice the sensor diameter. Finally, it is important to add a discharge resistor. The resistor must be connected between each electrode and the driven guard and earth to avoid a static charge and damage to the measuring sensor. Typically, the resistance value is 1 MΩ. If the capacitance of the inter-electrodes is around 1 pF, an earthed screen is required around the electrodes to avoid unwanted or external signals. Figure 10 shows a photo of the typically developed prototype.

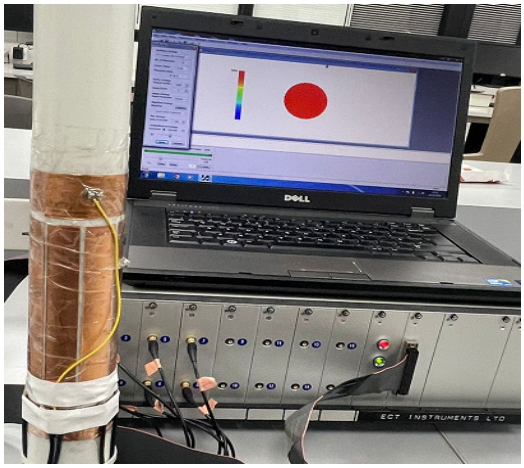

Fig. 10. A typical 8-electrode ECT sensor.

TABLE I. DIMENSIONS OF THE SENSOR PARTS

Component	Dimensions
Electrode dimensions= length×width	15×1.7 cm
Gap between electrodes	0.275 cm
External circumference of pipe	15.8 cm
Outer radius of pipe	2.51 cm
Inner pipe cross section area	19.86 cm^2
Total volume of the ECT section (electrode region): V_{total}= 19.86×15	297.9 cm^3

V. RESULT AND DISCUSSION

A. Sensitivity of Measurements

Two dielectric materials were used to calibrate the developed sensor: oil and air. Then, different amounts of oil were introduced into the pipe, where the air surrounded the oil. Figure 11 shows that the smallest amount to be detected had a cross-sectional area of 0.97 cm^2 (volume = 14.56 cm^3 and quantity = 0.67 L). A minimum detectable value was defined as the product of the dielectric constant to describe the *POS* sensitivity of the ECT sensor. The difference between the two dielectric materials (air and oil) was multiplied by the minimum detectable volume of the object and divided by the volume of the sensor section as in (6):

$$POS = \Delta\varepsilon_r \frac{V_{md}}{V_{total}} \times 100 \quad (6)$$

where *POS* is the percentage of sensitivity [20], $\Delta\varepsilon_r$ is the difference between the dielectric constants of the full and empty states, V_{md} is the minimum detectable volume of the object, and V_{total} is the total volume of the ECT Sensor. In the present case of oil $\Delta\varepsilon_r$ = 6. From Figure 10, the calculated sensitivity of the *POS* measurements was 67.4%. Figure 11 shows the decrease in the amount of oil gradually searching for the minimum detectable volume of the object V_{md}.

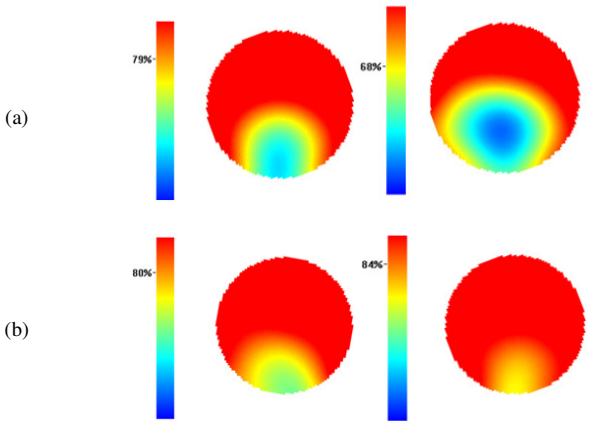

Fig. 11. Sensitivity patterns with variable amounts of different materials.

B. Accuracy of the Obtained Image

The accuracy of the measurements [21] was calculated from the images obtained. Two different dielectric materials were considered, where the empty state was air and the full state was lubricating oil (density = 823 kg/m^3). An amount of lubricating oil was introduced so that when the pipe was placed horizontally, it was half filled with lubricating oil. Referring to Figure 11, it was discovered that the separation line between the lubricating oil and the air deviated from being a sharp line. The gradual change from blue (air) to red color (lubricating oil) indicates that the accuracy of the sensor was not high enough. To quantify the accuracy of the ECT sensor, the percentage of accuracy (POA) was defined as follows:

$$\text{POA} = \left(1 - \frac{\text{line thickness}}{\text{Image diameter}}\right) \times 100 \quad (7)$$

The POA term was introduced to represent the percentage of accuracy. In the case of Figure 12, POA was achieved to be as high as 82%.

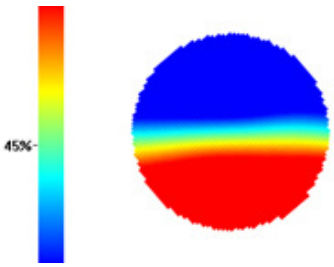

Fig. 12. Illustration of sensitivity pattern with two different materials when it is placed horizontally.

Figure 12 shows the line separation between the two different dielectric materials (lubricating oil and air) when the pipe is placed horizontally. The results obtained with the developed sensor with eight external electrodes show that the larger the width of the electrodes, the more accurate the measurements. Moreover, the shorter the electrode length, the more sensitive the measurements. These observations were made while keeping the same gap between the electrodes and for the same cross-sectional area.

VI. CONCLUSION

This paper presented the modeling, simulation, and experimental measurements of an ECT sensor having eight external electrodes. In terms of modeling, the potential distribution, the electric field, and the sensitivity map were obtained to extract the dependence of the sensor characteristics in terms of sensitivity and accuracy on the sensor parameters. To verify the modeling results, an 8-electrode ECT sensor was developed and implemented, and experimental measurements were carried out on two different materials filling the pipe with different proportions to determine the sensitivity of the measurements and the accuracy of the probe. Furthermore, definitions of accuracy and sensitivity were developed and calculated for the developed sensor to validate the simulation results.

ACKNOWLEDGEMENT

This project was funded by the National Plan for Sciences, Technology, and Innovation (MAARIFAH), King Abdulaziz City for Science and Technology, Kingdom of Saudi Arabia award number (14-ELE741-08).

REFERENCES

[1] K. J. Alme and S. Mylvaganam, "Comparison of Different Measurement Protocols in Electrical Capacitance Tomography Using Simulations," *IEEE Transactions on Instrumentation and Measurement*, vol. 56, no. 6, pp. 2119–2130, Sep. 2007, https://doi.org/10.1109/TIM.2007.908315.

[2] R. K. Rasel, S. M. Chowdhury, Q. M. Marashdeh, and F. L. Teixeira, "Review of Selected Advances in Electrical Capacitance Volume Tomography for Multiphase Flow Monitoring," *Energies*, vol. 15, no. 14, Jan. 2022, Art. no. 5285, https://doi.org/10.3390/en15145285.

[3] J. W. Park, J. M. Ha, H. M. Seung, H. Jang, and W. Choi, "Thickness evaluation of Cr coating fuel rod using encircling ECT sensor," *Nuclear Engineering and Technology*, vol. 54, no. 9, pp. 3272–3282, Sep. 2022, https://doi.org/10.1016/j.net.2022.03.035.

[4] Y. Tang, W. Lin, S. Xiao, K. Tang, and X. Lin, "A Measurement Compensation Method for Electrical Capacitance Tomography Sensors with Inhomogeneous Electrode Parameters," *Electronics*, vol. 11, no. 18, Jan. 2022, Art. no. 2957, https://doi.org/10.3390/electronics11182957.

[5] Z. Li, S. Xiao, Q. Yue, and T. Wang, "Electrical Capacitance Tomography Sensor With House Structure for Assisting Recognition of Objects," *IEEE Sensors Journal*, vol. 22, no. 5, pp. 4534–4544, Mar. 2022, https://doi.org/10.1109/JSEN.2022.3143709.

[6] R. Banasiak *et al.*, "Study on two-phase flow regime visualization and identification using 3D electrical capacitance tomography and fuzzy-logic classification," *International Journal of Multiphase Flow*, vol. 58, pp. 1–14, Jan. 2014, https://doi.org/10.1016/j.ijmultiphaseflow.2013.07.003.

[7] D. Chen, Y. Han, J. Huang, L. Wang, and X. Yu, "An Image Data Capture System for Electrical Capacitance Tomography of Oil/Water Two-Phase Flow," in *2006 IEEE International Conference on Information Acquisition*, Veihai, China, Dec. 2006, pp. 722–726, https://doi.org/10.1109/ICIA.2006.305817.

[8] Z. Cui, H. Wang, L. Tang, L. Zhang, X. Chen, and Y. Yan, "A Specific Data Acquisition Scheme for Electrical Tomography," in *2008 IEEE Instrumentation and Measurement Technology Conference*, Feb. 2008, pp. 726–729, https://doi.org/10.1109/IMTC.2008.4547132.

[9] Z. Cui *et al.*, "A review on image reconstruction algorithms for electrical capacitance/resistance tomography," *Sensor Review*, vol. 36, no. 4, pp. 429–445, Jan. 2016, https://doi.org/10.1108/SR-01-2016-0027.

[10] X. Dong and S. Guo, "Modelling an electrical capacitance tomography sensor with internal plate electrode," in *2009 International Conference on Test and Measurement*, Hong Kong, China, Sep. 2009, vol. 2, pp. 160–163, https://doi.org/10.1109/ICTM.2009.5413087.

[11] Z. Fan and R. X. Gao, "A new sensing method for Electrical Capacitance Tomography," in *2010 IEEE Instrumentation & Measurement Technology Conference Proceedings*, Austin, TX, USA, Feb. 2010, pp. 48–53, https://doi.org/10.1109/IMTC.2010.5488269.

[12] S. M. A. Ghaly, "LabVIEW Based Implementation of Resistive Temperature Detector Linearization Techniques," *Engineering, Technology & Applied Science Research*, vol. 9, no. 4, pp. 4530–4533, Aug. 2019, https://doi.org/10.48084/etasr.2894.

[13] Z. Guo, "New normalization method of imaging data for electrical capacitance tomography," in *2011 International Conference on Mechatronic Science, Electric Engineering and Computer (MEC)*, Jilin, China, Dec. 2011, pp. 1126–1130, https://doi.org/10.1109/MEC. 2011.6025665.

[14] A. Gupta, M. A. Abdelrahman, and W. A. Deabes, "A feature based solution to Forward Problem in Electrical Capacitance Tomography," in *2009 41st Southeastern Symposium on System Theory*, Tullahoma, TN, USA, Mar. 2009, pp. 49–53, https://doi.org/10.1109/SSST.2009. 4806824.

[15] S. M. A. Ghaly, K. A. Al-Snaie, M. O. Khan, M. Y. Shalaby, and M. T. Oraiqat, "Design and Simulation of an 8-Lead Electrical Capacitance Tomographic System for Flow Imaging," *Engineering, Technology & Applied Science Research*, vol. 11, no. 4, pp. 7430–7435, Aug. 2021, https://doi.org/10.48084/etasr.4122.

[16] S. Liu, L. Fu, and W. Q. Yang, "Optimization of an iterative image reconstruction algorithm for electrical capacitance tomography," *Measurement Science and Technology*, vol. 10, no. 7, Apr. 1999, Art. no. L37, https://doi.org/10.1088/0957-0233/10/7/102.

[17] N. Reinecke and D. Mewes, "Recent developments and industrial/research applications of capacitance tomography," *Measurement Science and Technology*, vol. 7, no. 3, Nov. 1996, Art. no. 233, https://doi.org/10.1088/0957-0233/7/3/004.

[18] L. Sheng, S. Yijian, and Z. Guibin, "Design of Data Acquisition System for 12-Electrode Electrical Capacitance Tomography," in *2007 International Conference on Mechatronics and Automation*, Harbin, China, Dec. 2007, pp. 2293–2297, https://doi.org/10.1109/ICMA.2007. 4303910.

[19] L. A. Abdulkareem, "Identification of Oil-Gas Two Phase Flow in a Vertical Pipe using Advanced Measurement Techniques," *Engineering, Technology & Applied Science Research*, vol. 10, no. 5, pp. 6165–6171, Oct. 2020, https://doi.org/10.48084/etasr.3679.

[20] Y. Yang, J. Jia, and H. McCann, "A faster measurement strategy of electrical capacitance tomography using less sensing data," in *2015 IEEE International Conference on Imaging Systems and Techniques (IST)*, Macau, China, Sep. 2015, pp. 1–5, https://doi.org/10.1109/ IST.2015.7294533.

[21] T. A. York, "Status of electrical tomography in industrial applications," *Journal of Electronic Imaging*, vol. 10, no. 3, pp. 608–619, Jul. 2001, https://doi.org/10.1117/1.1377308.